ChemPubSoc Europe

DOI: 10.1002/cctc.201500381

CHEMCATCHEM Minireviews

Viral Templated Palladium Nanocatalysts

Cuixian Yang and Hyunmin Yi*[a]

Palladium (Pd) nanocatalysis plays key roles in many areas from environmental remediation, energy utilization to chemical synthesis. Viruses offer exciting opportunities and advantages as promising nanoparticle synthesis templates due to their controlled dimensions and structures, and the ability to confer precisely spaced functionalities by genetic modification to permit improved and/or tunable metal nanoparticle formation. We have utilized tubular tobacco mosaic virus (TMV) as biologically derived nanotemplates for controlled synthesis of catalytically active Pd nanoparticles. Here we describe key findings and insights gained from our studies on the synthesis and characterization, as well as on both aqueous and organic phase catalytic reactions, dichromate reduction and the Suzuki-coupling reaction. We hope that the methodologies and results summarized here can spur further interdisciplinary collaboration, and expect that more discoveries and improved performances can be realized with future endeavors.

1. Introduction

Palladium (Pd) represents one of the most versatile and utilized noble metal elements in a vast array of catalytic reactions and applications,[1] such as organic coupling reactions,[2] hydrogenation of unsaturated olefins,[3] and alcohol oxidation.[4] Although homogeneous, ligand-associated forms of Pd catalysts are still widely used, heterogeneous nanocatalysts on high surface area supports are often preferred, owing to a number of advantages, including stability, simple catalyst recovery, and reuse. Yet, harsh and unpredictable catalyst synthesis conditions often involving high temperature calcination steps may pose limitations in developing a priori design principles, and/or achieving efficient generation and utilization of high activity catalytic surfaces, particularly in the case of colloidal nanoparticle catalysts prepared with capping agents.[5]

Historically regarded as harmful to humans, viruses have gained much attention in the past three decades as novel synthesis templates for metal, metal oxide, and other ceramic nanomaterials.[6] This attention is attributable to several inherent advantages, including highly controlled dimensions and structures in the nanoscale, diverse chemical functionalities from the rich repertoire of amino acids comprising the coat proteins, and the ability to impart additional functionalities with precise spacing and control via genetic modification. Except for animal viruses that pose biological hazard to humans and mammals, the vast majority of the viruses utilized for material synthesis are either bacterial or plant, and are deemed noninfectious once functionalized as their infection mechanisms and delicate self-assembly structures are disrupted at the molecular level. Although typically classified based on the nature of their genomes, various viruses can be grouped into three distinct shape categories from materials perspective: filamentous, icosahedral (spherical), and rigid rod-shaped.[6] Viruses in each category offer unique traits, and the applications and strategies for utilization have evolved around them.[7]

First developed by Smith,[8] random peptide libraries of the filamentous bacterial virus M13 offers an exciting and intriguing capability to screen for affinity to virtually any material of interest in an iterative screening process termed "biopanning".[9] Many research groups including the Belcher group have exploited this potent property for nanomaterial synthesis, and several types of functional inorganic nanomaterials have been synthesized on M13 viral templates, in some cases with promising properties for fuel cells,[10] lithium ion batteries[11] and photocatalytic applications.[12] Particularly, Knecht and co-workers utilized this biopanning technique to identify a peptide sequence (TSNAVHPTLRHL) with affinity for Pd, and synthesized small and uniform (1.9 ± 0.3 nm) Pd nanoparticles using short peptides for Stille coupling reaction.[13] A recent report by Belcher and co-workers reported substantially improved catalytic performance of lithium-oxygen batteries with the addition of low content Pd.[14]

Viruses belonging to the icosahedral shape category have also been extensively examined; for example, a series of pioneering works by Douglas and Young have exploited the precise inner capsid size and the pH-responsive swelling properties of plant viruses for the synthesis of various materials, including photocatalytically active titania nanoparticles.[15]

Some of the most important pioneers in the viral nanotechnology field are Kern and his coworkers, who have long utilized tobacco mosaic virus (TMV), the central biotemplate of this article, for the synthesis of a wide range of metal and inorganic nanomaterials including 3 nm diameter copper wires.[16] Our studies on TMV-templated Pd nanocatalysts are much inspired by their works,[17] as well as those of Culver and

[a] Dr. C. Yang, Prof. H. Yi
Department of Chemical and Biological Engineering
Tufts University, 4 Colby St. Medford, MA 02155 (USA)
E-mail: hyunmin.yi@tufts.edu

This publication is part of a Special Issue on Palladium Catalysis. To view the complete issue, visit:
http://onlinelibrary.wiley.com/doi/10.1002/cctc.v7.14/issuetoc

Harris,[18,19] as further described below. Our objective here is to offer a focused discussion on the key findings and encouraging results on the preparation, characterization, catalytic activity and stability of TMV-templated Pd nanocatalysts, not to provide a comprehensive overview or survey of the now rich viral and bioinspired nanobiotechnology field. As such, many inspiring works from pioneers such as Stubbs and Mann, as well as studies on other important materials for catalytic applications, are regretfully omitted in this work. Elegant review articles in the general field,[20] as well as in-depth molecular and mechanistic descriptions of bioinspired Pd and other catalysts can be found elsewhere.[21] In the following Section 2, we describe our earlier synthesis and characterization efforts via small angle X-ray scattering (SAXS) and other techniques. In Section 3, we summarize results on the catalytic activity and stability studies on dichromate reduction reaction, with particular attention to the new insights we gained on the reaction mechanisms, synthesis parameters and the role and utility of TMV templates for improved synthesis and fabrication. In Section 4, we offer the lessons learned from our study on Suzuki coupling reaction, followed by our recent reports on the integration of catalytically active Pd-TMV nanocomplexes into shape-controlled polymeric microparticle platforms via rapid microfluidic and robust replica molding schemes in Section 5.

2. Controlled Synthesis and Characterization of Pd Nanoparticles Formed on TMV Templates

TMV is a biologically derived nanotube that offers many unique properties and advantages for catalytic Pd nanoparticle synthesis. As the first discovered virus, a naturally occurring wild-type TMV consists of 2130 identical coat proteins (16.7 kDa) helically wrapped around a single-strand 6.4 kb mRNA genome, making up a rigid 300 nm length, 18 nm diameter nanotube with a 4 nm diameter inner channel.[22] Such highly defined structure, safety (i.e. non-infectious to mammalian cells), extraordinary stability (e.g. ≈90 °C, pH 2–10, various high concentration organic solvents, etc.), and simple mass production are only a few of the advantages that make TMV a potent nanotemplate that can be readily functionalized to generate high capacity functional materials. Importantly, Culver and colleagues genetically displayed cysteines (one buried in wtTMV) near outer surfaces of TMV coat proteins (TMV1cys and TMV2cys), as shown in the Chimera model of TMV in Figure 1 (a), and reported improved metal precursor adsorption and Pd nanoparticle formation.[19,23,24] In many of our earlier works, we utilized enhanced surface-adsorption of TMV1cys on gold substrates via gold–thiol binding for high density surface assembly of TMV, followed by Pd nanoparticle synthesis by simple reduction of Pd precursor sodium tetrachloropalladate (Na_2PdCl_4) with mild reducing agents such as sodium hypophosphite ($NaPH_2O_2$) as shown in the schematic diagram of Figure 1 b.[25]

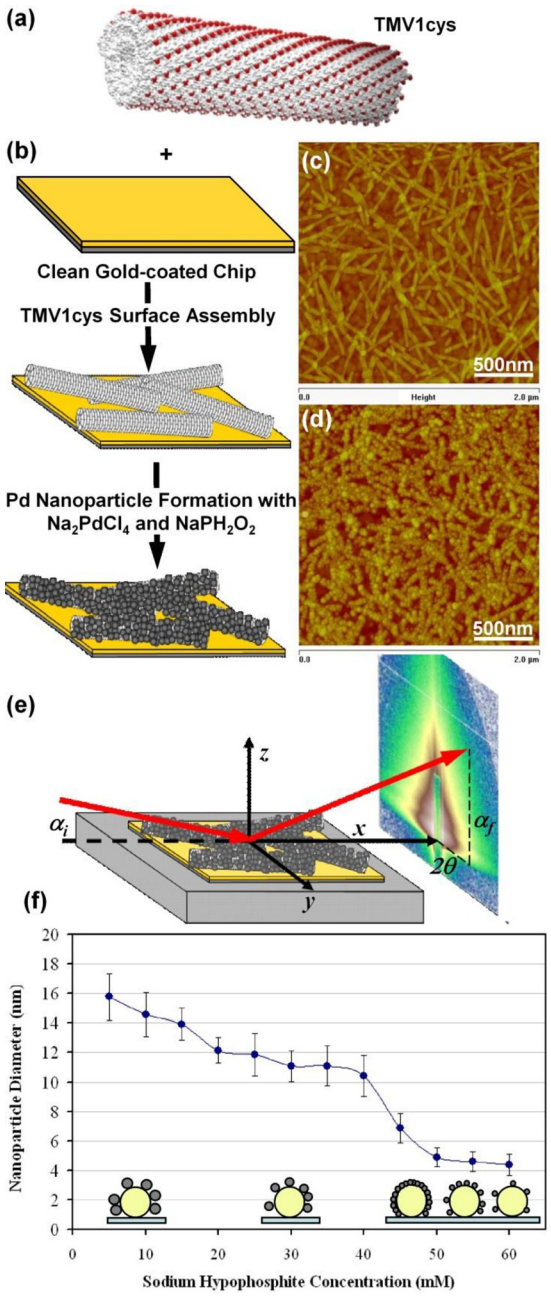

Figure 1. Controlled synthesis of Pd nanoparticles on surface-assembled TMV templates. a) Chimera model of a fraction of TMV1cys showing genetically displayed cysteines in red. b) Schematic diagram showing surface assembly followed by Pd nanoparticle formation. c) AFM image of surface-assembled TMVs. d) Pd nanoparticles preferentially formed along TMV templates. e) Schematic diagram of GISAXS setup. f) Pd nanoparticle sizes vs. sodium hypophosphite concentrations. Adapted from Ref. [25]. Copyright (2010) American Chemical Society.

2.1. Grazing Incidence Small-angle X-ray Scattering (GISAXS) for Examination of Controlled Pd Nanoparticle Synthesis

As shown in the atomic force microscopy (AFM) image of Figure 1 c, simple exposure of clean gold surfaces to aqueous TMV solution leads to high density and preferential surface-assembly of TMV rising from the thiol groups genetically displayed near the outer edge of each coat protein.[25] Next, high

density of Pd nanoparticles along the TMV's nanotubular structures are readily achieved in a consistent and controlled manner under mild aqueous conditions, as shown in Figure 1 d. To overcome AFM's inherent size overestimation and to examine the influence of synthesis parameters on the particle size, we performed a series of grazing incidence small-angle X-ray scattering (GISAXS) experiments at the Advanced Photon Source (beamline 12 ID-C) of Argonne National Laboratory.[25] In a typical GISAXS setup (Figure 1 e), planar or surface-assembled samples are irradiated with a monochromatic X-ray beam at a grazing angle (e.g. $\alpha_i = 0.1^\circ$ in most of our studies),[25] the X-ray scattered at small angle recorded on a 2D detector as a function of the scattering angle (2θ in the horizontal direction and α_f in the vertical direction). A rich pool of information ranging from the nanostructure morphology to precise dimensions can be extracted over a large sample area, giving statistically meaningful information (see Supporting Information for a short tutorial and Guinier analysis in Manocchi et al.).[26] Upon thorough examination of several reducing agents, we observed that sodium hypophosphite yields controlled synthesis of Pd nanoparticles in 4–16 nm diameter range by simply changing the reducer concentration as shown in Figure 1 f, where higher concentrations of reducer result in smaller Pd nanoparticle formation. In short summary, this first study established a simple and controlled Pd nanoparticle synthesis Scheme on TMV templates in a surface-assembled format, along with in-depth characterization methods on particle size and nanostructures via the GISAXS technique.

2.2. High Thermal Stability of Pd-TMV Nanocomplexes

GISAXS is indeed a potent technique that allows rapid in situ examination of nanoscale structures (typically 1–60 nm feature sizes) and their dynamic behavior in an accurate, statistically meaningful and non-destructive manner unlike TEM. In the next set of studies, we exploited these traits to examine thermal stability of the Pd nanoparticle-TMV complexes in an in situ GISAXS format.[25] Briefly, various samples with surface-assembled TMVs with or without small (4 nm) to large (16 nm) Pd nanoparticles were mounted on a heater, and GISAXS patterns were recorded and analyzed by means of Guinier analysis upon programmed heating at $5\,^\circ C\,min^{-1}$. As illustrated in the representative scattering patterns in Figure 2 a, randomly aligned TMVs on surfaces with their monodisperse nanotubular dimensions generate strong scattering in the vertical (α_f) direction, with the characteristic oscillations typical of monodisperse nanotubular objects.[26] As heating progresses, the loss of such scattering pattern at 197 °C indicates degradation of TMV's nanotubular structure. In comparison, Pd-TMV complexes yield strong isotropic scattering in the horizontal direction that is largely maintained upon heating, until sudden disappearance occurs at relatively well-defined temperatures, as partially illustrated in Figure 2 b and c. Importantly, further line-cut plot, normalized scattering intensity and Guinier analyses all revealed that the Pd-TMV nanostructures have substantially higher thermal stability than TMV or Pd nanoparticles grown on the plain gold substrates. Specifically, Pd-TMV complexes

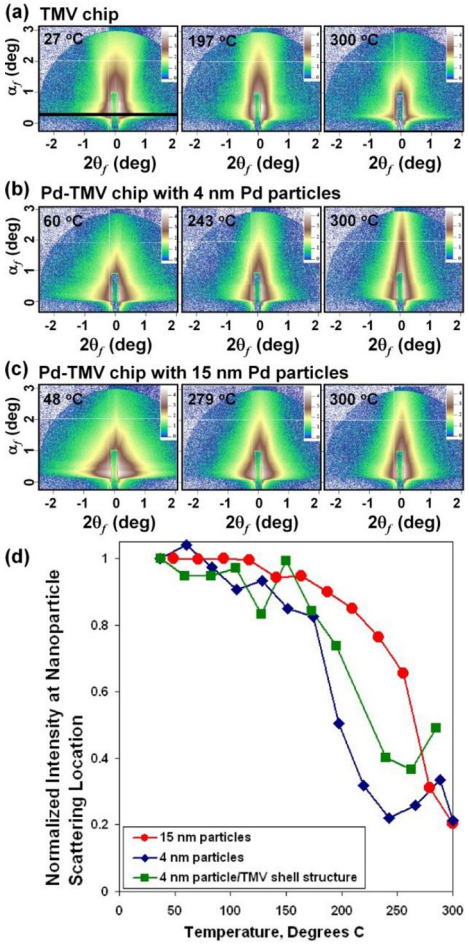

Figure 2. Thermostability of surface-assembled Pd-TMV complexes. GISAXS images at lower (leftmost column), critical transition/collapse (middle) and complete degradation (rightmost) temperatures of a) TMV, b) 4 nm Pd-TMV and c) 15 nm Pd-TMV nanocomplexes. d) Normalized scattering intensity plot showing degradation at varying temperatures. Adapted from Ref. [26]. Copyright (2010) American Chemical Society.

with 4 nm Pd particles showed stability in their overall nanostructure and nanoparticle density up to 243 °C, while the complexes with 15 nm Pd particles were stable up to 279 °C.[26] Along with the simultaneous degradation of TMV and Pd nanoparticles observed through these studies, we hypothesized that the TMV and the Pd nanoparticles grown on them provide synergistic enhancement in the thermal stability. Although the inherent lack of chemical and thermal stability of biotemplates are of concern for catalytic applications, the high thermal stability of Pd-TMV nanocomplexes observed in this GISAXS study showed potential for our approach.

2.3. Fundamental Role of TMV Templates in Pd Nanoparticle Formation via in situ SAXS

Further exploiting the capability of the SAXS technique to examine dynamic behavior of nanoscale objects, we next carried out a series of in situ Pd nanoparticle formation experiments with TMV templates in a bulk solution format, as shown in the schematic diagram of Figure 3 a.[27]

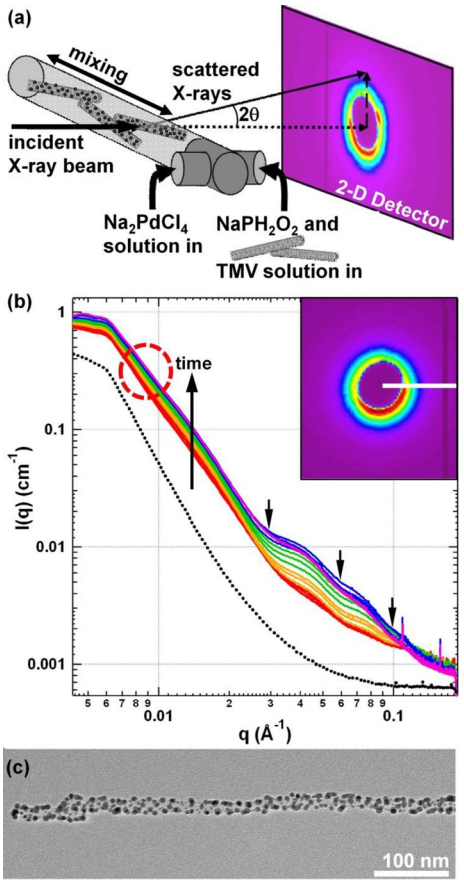

Figure 3. In situ SAXS-based examination of Pd nanoparticle formation on TMV templates. a) Schematic diagram of the in situ SAXS setup. b) Representative SAXS line-cut plot of Pd nanoparticle formation on TMV templates. c) Representative TEM image of the Pd-TMV complex formed under the condition in b). Adapted from Ref. [27]. Copyright (2011) American Chemical Society.

Briefly, separate aqueous solutions containing the Pd precursor (Na_2PdCl_4) and the reducer ($NaPH_2O_2$) with TMV were mixed in a quartz capillary, and 2D SAXS images over two minute periods were recorded and analyzed. The representative line-cut plot of scattering intensity [*I*(q)] over scattering vector q in Figure 3b illustrates several important findings. First, TMV's highly monodisperse nanotubular structure coated with electron-dense Pd nanoparticles gives rise to characteristic oscillating patterns as indicated with three small arrows. The scattering intensity continues to rise as Pd particles grow, while the overall oscillation patterns do not change over time, indicating the retention of TMV's monodisperse structures. Particularly, the local minima continue shifting to the low q range over time, indicating enlargement of the tubular diameter of the Pd-TMV complexes as Pd particles continue to grow (i.e. inverse correlation between scattering object's size and the scattering angle in Bragg's law).[27] Finally, the increasing scatting intensity in low q region (dashed circle) clearly indicates that particles are formed on TMV templates and not in the bulk solution. This important observation is in good agreement with the findings of Lim et al.,[24] who showed much enhanced adsorption (two-fold) of Pd precursors on TMV1cys over wtTMV stemming from the genetically displayed cysteine residues. In short summary, this in situ SAXS study revealed fundamental roles of TMV as a potent nanotemplate for enhanced precursor adsorption and preferential growth of Pd nanoparticles.

3. TMV-templated Pd Nanocatalysts for Dichromate Reduction

Hexavalent chromium (Cr^{VI}, dichromate) is a prevalent industrial pollutant in waste sites and drinking water sources, and known to possess carcinogenic and mutagenic properties.[28] Catalytic reduction of dichromate to nontoxic chromate (Cr^{III}) represents a promising alternative for environmental remediation and water pollution control. We have utilized this simple surface-originated liquid phase electron transfer reaction to examine the catalytic activity of Pd nanoparticles grown on TMV templates in various formats.

3.1. Viral-templated Pd Nanocatalysts in Surface-assembled Format

Our first report on the catalytic activity of TMV-templated Pd nanoparticles utilized the simple surface-assembled format as shown in Figure 4a. Briefly, TMV was first self-assembled on the gold-coated substrates by simply dipping in aqueous TMV1cys solution. These TMV chips are then immersed into aqueous Pd precursor solution with mild reducing agent to

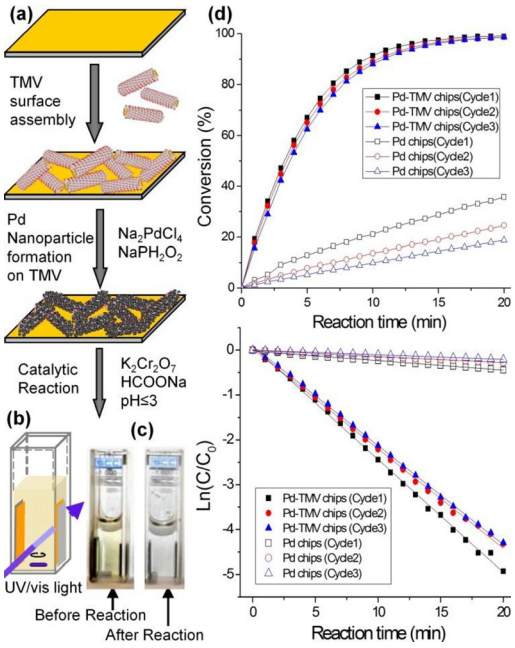

Figure 4. Catalytic activity and reusability of Pd nanoparticles formed on surface-assembled TMV templates for dichromate reduction reaction. a) Schematic diagram of Pd-TMV chip fabrication. b) Schematic diagram of a batch reaction in a quartz cuvette with a Pd-TMV chip and in situ monitoring via UV-vis. c) Photographs of the reaction mixtures before and after the dichromate reduction reaction. d) Conversion and apparent pseudo-first order rate constants over three repeated batch reactions with one Pd-TMV chip. Adapted from Ref. [28] with permission from Elsevier.

form 11–12 nm Pd nanoparticles along TMV templates. As shown in the schematic diagram of Figure 4b and the photographs of Figure 4c, this surface-assembly scheme allowed the catalysts in a chip-based format to be directly dipped in the reaction solution containing dichromate and the electron donor formic acid. The catalytic reactions were then monitored in real time via simple in situ UV/vis spectrophotometry by measuring absorbance at dichromate's characteristic absorption peak at $\lambda = 350$ nm.[28] By simply taking the logarithm of the conversion, the apparent pseudo-first order rate constant of dichromate reduction with Pd-TMV catalysts was readily determined to be 0.2518 min^{-1} (Figure 4d). This chip-based format also enabled simple catalyst recovery (i.e. taking out the chips from the reaction mixtures) and reuse; 88% of Pd-TMV catalyst's reactivity was retained upon three repeated batch reactions without any regeneration treatment, whereas Pd on gold surface without TMV templates showed rapid decline (52%) in the reaction rate (Figure 4d). AFM and GISAXS measurements showed that the overall average size of Pd nanoparticles does not change significantly upon three recycled reactions, which further indicated the stability of the Pd-TMV complexes under the reaction conditions in our study (e.g., pH 3.0).[28]

X-ray photoelectron spectroscopy (XPS) also showed no meaningful changes in the chemical state with no significant decomposition of the Pd-TMV complexes or leaching of Pd nanoparticles into the reaction solution. Although we didn't examine turnover frequency (TOF) or other quantitative parameters in this first work (further examined in Section 3.3),[29] this work demonstrates the dual functionality and utility of TMV templates in enhanced surface assembly and catalytically active Pd nanoparticle formation, as well as the stability to maintain Pd catalysts well-dispersed through multiple reaction cycles.

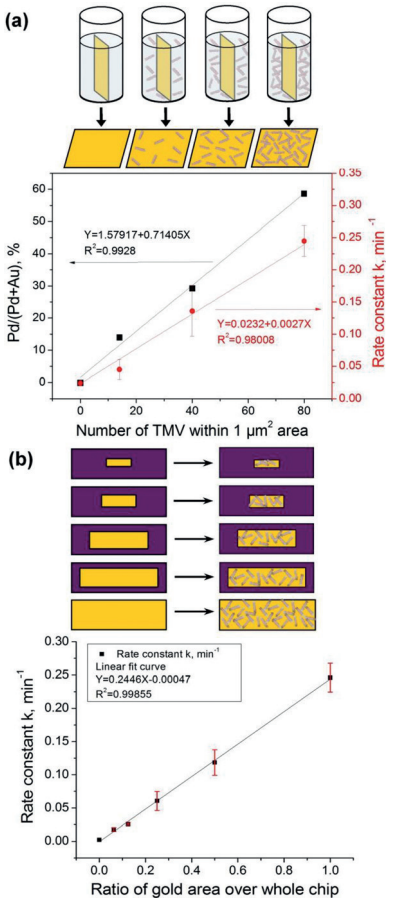

Figure 5. Tunable and spatially controlled formation of Pd nanocatalysts on surface-assembled TMV Templates. a) Schematic diagram of the TMV concentration-based surface loading control, and Pd loading density and rate constant plot vs. TMV surface density. b) Schematic diagram of patterned surface area-based control of Pd-TMV complexes, and a rate constant plot vs. surface area. Adapted from Ref. [30] with permission from Elsevier.

3.2. Tunable and Programmable Surface Assembly of Pd-TMV Nanocomplexes

Owing to the genetically displayed cysteines, TMV1cys can be utilized for tunable and preferential surface assembly. In the next study, we exploited this property to develop two simple routes in tuning the surface loading density and location of TMV-templated Pd nanocatalysts on gold chips that are otherwise highly challenging in traditional microfabrication techniques as shown in Figure 5.[30] In the first approach (Figure 5a), the TMV surface coverage density was tuned by simply varying the TMV concentration for assembly onto gold substrates. Pd nanoparticles were selectively formed along TMV templates only, and the resulting total Pd surface loading density (XPS) as well as the reaction rate constant for dichromate reduction showed linear relationship with TMV surface density.

In the second approach (Figure 5b), gold-patterned chips with varying gold surface areas were fabricated by a standard photolithographic patterning technique for the spatial control of Pd-TMV catalysts. As TMVs were preferentially assembled on gold, but not on silicon nitride (AFM), the catalytic activity from patterned chips with different sizes of gold areas correlated linearly with the gold surface area. This linear relationship between the rate constant and the area of gold patterns clearly indicates the simple spatial control and patterned synthesis of Pd nanocatalysts permitted by TMV's selective surface assembly and preferential Pd nanoparticle formation as enabling bioengineered templates.

3.3. Catalytic Reaction Kinetics and Tunable Catalyst Synthesis

Recently, we further examined the dichromate reduction mechanism and synthesis–structure–activity relationship of TMV-templated Pd nanocatalysts in this surface-assembled format as shown in Figure 6.[29] It was found that the reaction kinetics of dichromate reduction follows a Langmuir–Hinshelwood mechanism (Figure 6a), which involves competing surface adsorption of dichromate and formic acid on the active surface of Pd nanoparticles. The adsorption of dichromate onto the Pd nanocatalyst surface was shown to be substantially stronger ($\approx$300 times) than that of formic acid. By simply tuning the concentrations of the Pd precursor and reducer during the syn-

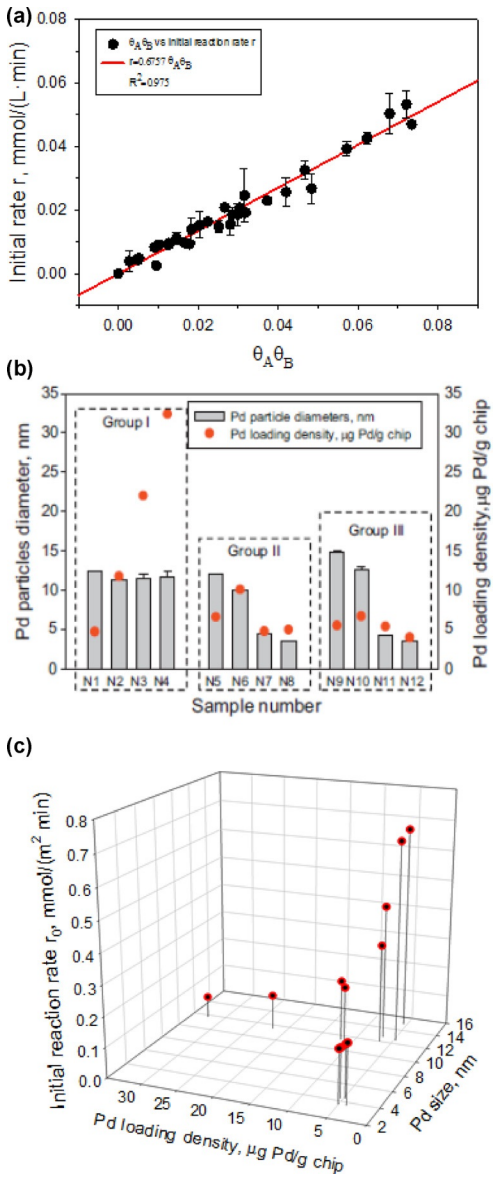

Figure 6. Catalytic reaction kinetics and tunable catalyst synthesis. a) Langmuir-Hinshelwood mechanism of dichromate reduction, and an initial rate plot vs. $\theta_A\theta_B$ (θ represents surface coverage of reactants). b) Effect of synthesis conditions on the Pd particle size and surface loading density. c) 3D bar chart of catalytic reactivity vs. catalyst structure Pd size and loading density). Adapted from Ref. [30] with permission from Elsevier.

thesis procedure, Pd nanoparticle size, catalyst loading density and catalytic activity of viral templated Pd catalysts were readily controlled, as shown in Figure 6b. Increase in Pd precursor concentration at the same reducer concentration resulted in higher Pd loading density, whereas higher reducer concentration at the same Pd precursor concentration led to formation of smaller Pd nanoparticles. Under optimized synthesis condition, TMV-templated Pd nanocatalysts exhibited 68% higher catalytic activity per unit Pd mass in comparison with commercially available 5% Pd/C catalysts, suggesting the advantage of TMV templates in the synthesis of Pd nanocatalysts with pristine surfaces for higher catalytic activity due to the absence of capping agents to maintain the dispersed states. In addition, we found size-dependent behavior with Pd-TMV chip catalysts, that is, catalysts with larger Pd particle size and lower Pd loading density led to higher catalytic activity per unit Pd surface area (Figure 6c).

4. TMV-templated Pd Nanocatalysts for Suzuki Coupling Reaction

Owing to the mild reaction conditions and ready availability of precursors, the Pd-catalyzed Suzuki–Miyaura C–C cross-coupling reactions are extensively utilized to synthesize biaryl compounds (Figure 7a).[31] We enlisted our surface-assembled Pd-TMV complexes in the chip-based format (Figure 4a) to examine the catalytic activity and a number of important parameters in this Suzuki reaction.[32] Specifically, we carried out several sets of small scale batch reaction experiments primarily with phenylboronic acid and iodoanisole (Figure 7a) to determine optimal reaction conditions, reaction yields, selectivity, catalyst stability, and recyclability, as well as reaction mechanism in the ligand-free semi-heterogeneous format. We were able to achieve complete conversion to the desired cross-coupling product methoxy biphenyl under mid conditions in a mixture of acetonitrile and water at 50 °C. Our simple chip-based format enabled simple catalyst separation and reuse (Figure 7b), facile product recovery and reaction mechanism studies.

In particular, the solvent ratio played an important role in the selectivity of the Suzuki reaction, where a higher water/acetonitrile ratio significantly facilitated the cross-coupling pathway, and suppressed the homo-coupling reaction (Figure 7c), presumably due to the enhanced solubility and accessibility of base to activate the iodoanisole and boronate species required for the transmetalation step in the reaction mechanism.[33,34] The reactant content ratio study (Figure 7d) showed that higher aromatic boronic acid content than iodoanisole in the reactant mixture enhanced the completion of the cross-coupling reaction, while a certain amount of aromatic boronic acid followed the homocoupling pathway.[34] The Pd loading applied for each batch reaction is 0.15 mol% based on the based on aryl halide, which is lower than in other heterogeneous catalyst systems; for example, 0.3 mol% for Pd/C,[35] 2.5 mol% for Pd/zeolite,[36] and 0.5 mol% for Pd/Chitosan.[37]

Importantly, a simple chip removal experiments along with ICP-OES analysis enabled us to further explore the reaction mechanism (i.e. active catalyst species) for the Suzuki reaction; the reaction continued to proceed to completion even after the Pd-TMV chip was removed unlike the dichromate reduction that originates entirely from the competitive adsorption of dichromate and formic acid onto the Pd surfaces[29] (see also Supporting Information in Yang et al.).[32] We found that Suzuki reactions were catalyzed largely by trace amounts of Pd species (1–90 ppb) that are leached into the reaction solution, and not on the solid catalyst surface, consistent with findings in other studies.[38] In sum, our simple surface-assembled chip-based format served as the pre-catalyst pool for stable, readily recyclable and efficient catalyst platforms for Suzuki coupling

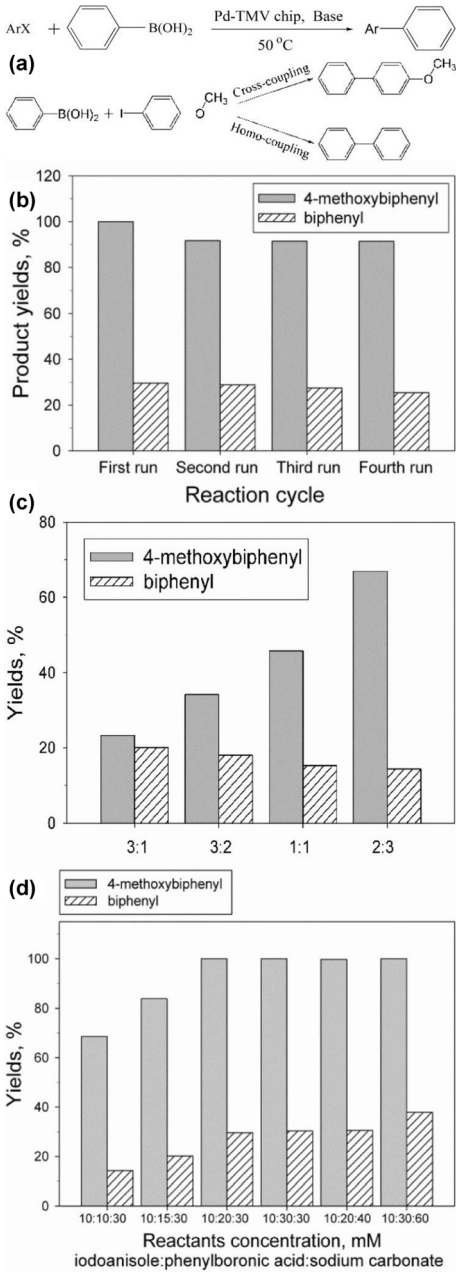

Figure 7. Viral-templated Pd nanocatalysts for Suzuki-coupling reaction. a) Scheme of Suzuki cross- and homo-coupling reactions catalyzed by nanostructured Pd-TMV complexes. b) Recycling test of Pd-TMV chip-catalyzed Suzuki reaction. c) Effect of solvent CH_3CN/H_2O volume ratio on reaction selectivity. d) Effect of reactant ratios on product yields. Adapted from Ref. [32] with permission from The Royal Society of Chemistry.

reaction that further enabled studies on a number of important reaction parameters.

5. Integration of Catalytically Active Pd-TMV Nanocomplexes with Polymeric Microparticles

5.1. Rapid Microfluidic Fabrication of Catalytically Active Hydrogel Microparticles

Microfluidic techniques have gained substantial attention for fabrication of microscale polymeric materials owing to several advantages, including rapid processes, uniform dimensions of the resulting materials and the ability to confer multiple functionalities in spatially discrete domains.[39] In our first attempt to capture the catalytic activity of Pd-TMV nanocomplexes synthesized in aqueous solutions (Figure 3)[27] in readily deployable polymeric hydrogel formats, we enlisted a simple two-phase flow Scheme to manufacture polyethylene glycol (PEG)-based microparticles containing Pd-TMV complexes in collaboration with Patrick Doyle's group, as shown in Figure 8.[40] As shown in the schematic diagram of Figure 8a and the micrograph of Figure 8b, aqueous microflows containing the polymerizable PEG diacrylate and Pd-TMV complexes are continuously split into droplets and cross-linked to form microparticles via photoinduced radical polymerization of the acrylates. Owing to the laminar nature of the microfluidic flows, one can readily introduce multiple functionalities into single microparticles, in our study Janus particles containing one domain with Pd-TMV complexes for catalytic activity and the other with iron oxide nanoparticles for simple magnetic separation (Figure 8c–e). The loading density and catalytic activity of the Pd-TMV complexes (comparable to or higher than surface-assembled ones) encapsulated in the polymeric microparticles were also readily tunable, as shown in the rate constant plot of dichromate reduction in Figure 8f.

In sum, a simple microfluidic fabrication was shown to be effective in capturing the catalytically active Pd-TMV complexes in hydrogel microparticle formats where the reactants were permitted ready access to the catalytic sites.

5.2. Integration of TMV-templated Small Pd Nanocatalysts with Polymeric Microparticles via Robust Replica Molding

Our TMV-templated Pd nanocatalysts consistently showed comparable or higher specific catalytic activities to standard Pd/C catalysts due to the pristine, capping agent-free nature despite relatively larger particle sizes (4–11 nm diameter) rising from the use of sodium hypophosphite reducer.[29] Smaller particle sizes, however, offer inherent advantages of larger surface area per unit mass of precious Pd metal. Inspired by Lim et al.'s study on Pd coating of TMV templates in the absence of external reducer,[41] we recently examined spontaneous formation of Pd nanoparticles under elevated temperature and observed consistent formation of small (1–2 nm), uniform and highly crystalline Pd nanoparticles along TMV1cys.[42] We then enlisted a simple and robust replica molding technique to encapsulate the Pd-TMV complexes in a stable and shape-encoded PEG-based polymeric microparticle format (Figure 9).

In the synthesis step **1** of our integrated synthesis-fabrication approach (Figure 9a), TMV was simply mixed with the Pd

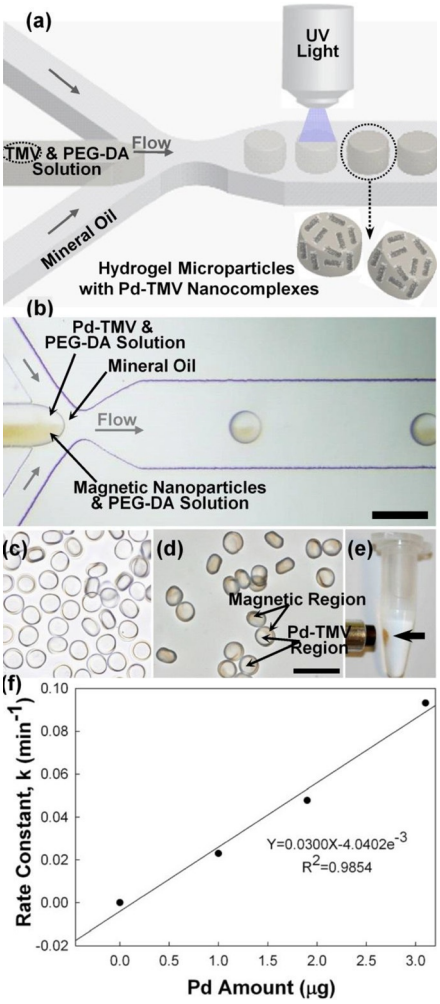

Figure 8. Microfluidic fabrication of polymeric hydrogel microparticles containing Pd-TMV complexes. a) Schematic diagram of a two-phase flow-focusing microfluidic device. b) Photomicrograph of a microfluidic channel with two PEGDA solution-based prepolymer fluids containing Pd-TMV and magnetic nanoparticles in each. Scale bars represent 100 μm. c) PEG hydrogel microparticles containing Pd-TMV complexes. d) Janus microparticles containing Pd-TMV and magnetic nanoparticles in each domain. e) Photograph showing magnetic separation of the Janus particles in (d). f) Apparent rate constant plot of microparticles in c) vs. Pd nanoparticle loading amount. Adapted from Ref. [40] Copyright (2010) American Chemical Society.

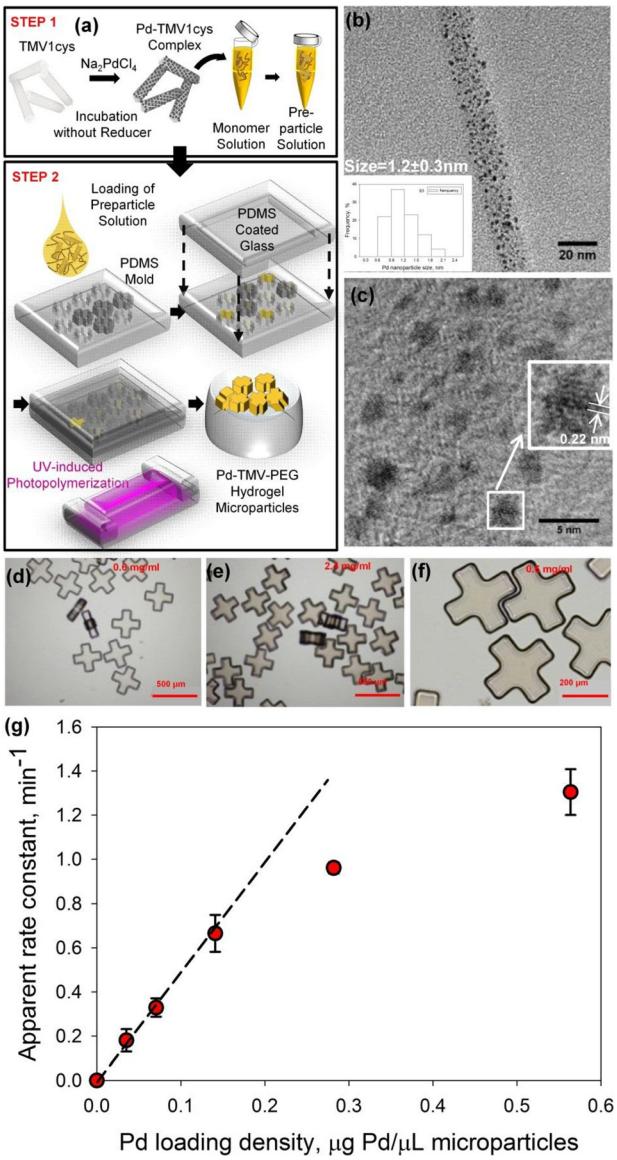

Figure 9. Integration of catalytically active Pd-TMV nanostructures into polymeric hydrogel microparticles via replica molding. a) Synthesis of Pd-TMV complexes and encapsulation into PEG microparticles by Replica Molding. b,c) TEM images of small Pd nanoparticles along TMV templates. d–f) Photomicrographs of the fabricated Pd-TMV-PEG microparticles. g) Plot of Pd loading densities in Pd-TMV-PEG microparticles vs. apparent reaction rate constants. Adapted from Ref. [42]. Copyright (2013) American Chemical Society.

precursor (Na_2PdCl_4) solution at 50 °C for 30 min to form the Pd nanoparticles well-dispersed along TMV surface (Figure 9b) with near-complete conversion without any reducer. The Pd nanoparticles formed on TMV templates are highly crystalline (Figure 9c), showing (111) facet of the face centered cubic (FCC) structure of metallic Pd crystals. Intriguingly, the as-prepared Pd-TMV complexes formed randomly networked TMV architectures. This was attributed to the screening of repulsive forces among negatively charged amino acids that confer the rigidity to TMV, and led to readily recoverable (i.e. simple precipitation by spin-down) and stable (i.e. readily re-dispersed) forms. In the fabrication step **2**, the Pd-TMV complexes were mixed with PEG diacrylate (PEGDA) and photoinitiator to yield the preparticle solution then placed on PDMS micromolds. Cross-linked PEG-based hydrogel microparticles containing the Pd-TMV complexes were formed upon photo-induced polymerization with a simple hand-held UV lamp. As shown in Figure 9d–f, the photomicrographs of the Pd-TMV-PEG microparticles have uniform color, shape and highly consistent dimensions without any apparent aggregation or deformation.

Particularly, the Pd density inside microparticles can be readily tuned in a range of 0.035–0.56 μg Pd/μL microparticles simply by changing the loading density of the Pd-TMV complexes in the preparticle solution. The fabricated Pd-TMV-PEG microparticles were applied for dichromate reduction, and showed 6-fold higher catalytic activity per Pd mass than the commercial Pd/C catalyst. The apparent reaction rate constant

is proportional to the Pd loading density in the kinetic controlled regime indicating ready access of the reactants to catalyst sites through polymer networks (25% PEG), then levels off in the higher Pd-TMV loading density cases as slight internal diffusion limitation was present (Figure 9(g)). In addition, recycle and long term storage (2 weeks) experiments showed minimal decrease in catalytic activity including the retention of the microparticle dimensions, clearly indicating the utility and stability of our polymeric hydrogel microparticle-based encapsulation strategy.[42]

The high catalytic activity, stability and recyclability of the Pd-TMV PEG microparticles as catalysts indicate retention of the Pd-TMV complexes within the polymeric networks due to the relative dimensions of Pd nanoparticles (1–2 nm), networked Pd-TMV complexes (up to micrometers), hydrogel mesh size (≈2–3 nm), and small molecule reactants and products (Å's). On one hand, the integration of 1–2 nm Pd nanoparticles with TMV nanostructures (300 nm length) allows Pd nanoparticles to remain well-dispersed on networked TMV superstructures and entrapped inside the hydrogel networks under catalytic reaction conditions. On the other hand, the 2–3 nm mesh size of hydrogel allows minimal mass transfer limitation of small molecule reactants and products through microparticles with the 50 μm characteristic diffusion length (i.e. 100 μm microparticle size) examined in this study. Hence, TMV biotemplates enable the synthesis, dispersion and retention of small Pd nanoparticles within the PEG hydrogel network structure. Furthermore, the microparticle size and mesh size can be readily controlled and manipulated for optimal payload of Pd nanoparticles and catalytic performance.

6. Conclusions and Future Perspectives

In this report, we described key procedures and findings on the synthesis, characterization and fabrication of TMV-templated Pd nanocatalysts in various formats. The robust and precise structures, along with the genetically displayed cysteines of TMV templates enabled efficient synthesis of Pd nanocatalysts in the wide size ranges under mild aqueous conditions as well as assembly into both surface-assembled and hydrogel-embedded formats. Through surface-originated dichromate reduction and leaching-based Suzuki coupling reaction, the as-prepared Pd nanocatalysts showed promising activity, stability and reusability.

Despite these encouraging results, there remain several aspects for further development and improvement in our viral-templated Pd nanocatalysis approach. The inherent lack of stability of biological templates under harsh, oxidizing, strong acidic (pH < 2) or basic (pH > 10), and/or higher temperature reaction conditions despite TMV's unusually robust and stable structures could be addressed in a number of ways, while our chip-based Pd-TMV complexes showed excellent stability for a range of Suzuki coupling reaction conditions.[32] Simple coating with mesoporous silica and/or hollow carbon rods is currently under investigation. Since the TMV's overall structure is primarily comprised of non-covalent self-assembly of the coat proteins, TMV could also serve as a sacrificial template to provide disassembled coat protein-based peptides for controlled nanoparticle synthesis under certain conditions. We have in fact had a recent success on the synthesis of small (≈2 nm) and uniform silver nanoparticles with high pH Tollen's reagent that showed high catalytic activity and stability for *p*-nitrophenol reduction reaction.[43] Similar approaches as well as genetic modifications to introduce other amino acids or peptides could be envisioned for further improvement in the controlled synthesis of other catalytic materials; ample information and precedents exist in the literature on peptide-based and related approaches.[44] Controlled synthesis of alloys, sub-nanometer clusters and core-shell catalysts for improved selectivity, as well as multicomponent systems for multistep, complex reaction systems are only a few of several active areas in a broader perspective; of an important final note are the continuing endeavors of the Belcher group for a wide range of application areas in this regard.[14,45]

Acknowledgements

We would like to extend our special thanks to the collaborators that offered inspiration and significant contributions to the works described here; Dr. Byeongdu Lee and Dr. Soenke Seifert at Argonne National Laboratory, Professor Patrick S. Doyle at MIT, Professor Changsoo Lee at Chungnam National University and Dr. Chang-hyung Choi at Harvard University.

Keywords: nanobiotechnology · nanocatalysts · palladium · Suzuki coupling reaction · tobacco mosaic virus

[1] I. Saldan, Y. Semenyuk, I. Marchuk, O. Reshetnyak, *J. Mater. Sci.* **2015**, *50*, 2337–2354.
[2] N. Miyaura, A. Suzuki, *Chem. Rev.* **1995**, *95*, 2457–2483.
[3] a) Á. Molnár, A. Sárkány, M. Varga, *J. Mol. Catal. A* **2001**, *173*, 185–221; b) M. Studer, H.-U. Blaser, C. Exner, *Adv. Synth. Catal.* **2003**, *345*, 45–65.
[4] E. Antolini, *J. Power Sources* **2007**, *170*, 1–12.
[5] a) D. Astruc, F. Lu, J. R. Aranzaes, *Angew. Chem. Int. Ed.* **2005**, *44*, 7852–7872; *Angew. Chem.* **2005**, *117*, 8062–8083.
[6] T. Douglas, M. Young, *Science* **2006**, *312*, 873–875.
[7] J. M. Rego, H. Yi, *Supramolecular Chemistry*, Wiley, Hoboken, **2012**.
[8] G. Smith, *Science* **1985**, *228*, 1315–1317.
[9] J. M. Galloway, S. S. Staniland, *J. Mater. Chem.* **2012**, *22*, 12423–12434.
[10] Y. Lee, J. Kim, D. S. Yun, Y. S. Nam, Y. Shao-Horn, A. M. Belcher, *Energy Environ. Sci.* **2012**, *5*, 8328–8334.
[11] Y. J. Lee, H. Yi, W. J. Kim, K. Kang, D. S. Yun, M. S. Strano, G. Ceder, A. M. Belcher, *Science* **2009**, *324*, 1051–1055.
[12] Y. S. Nam, A. P. Magyar, D. Lee, J.-W. Kim, D. S. Yun, H. Park, T. S. Pollom, D. A. Weitz, A. M. Belcher, *Nat. Nanotechnol.* **2010**, *5*, 340–344.
[13] D. B. Pacardo, M. Sethi, S. E. Jones, R. R. Naik, M. R. Knecht, *ACS Nano* **2009**, *3*, 1288–1296.
[14] D. Oh, J. Qi, Y.-C. Lu, Y. Zhang, Y. Shao-Horn, A. M. Belcher, *Nat. Commun.* **2013**, *4*, 2756.
[15] M. T. Klem, M. Young, T. Douglas, *J. Mater. Chem.* **2008**, *18*, 3821–3823.
[16] S. Balci, A. M. Bittner, K. Hahn, C. Scheu, M. Knez, A. Kadri, C. Wege, H. Jeske, K. Kern, *Electrochim. Acta* **2006**, *51*, 6251–6257.
[17] M. Knez, M. Sumser, A. M. Bittner, C. Wege, H. Jeske, T. P. Martin, K. Kern, *Adv. Funct. Mater.* **2004**, *14*, 116–124.
[18] a) X. Chen, K. Gerasopoulos, J. Guo, A. Brown, C. Wang, R. Ghodssi, J. N. Culver, *ACS Nano* **2010**, *4*, 5366–5372; b) E. Dujardin, C. Peet, G. Stubbs, J. N. Culver, S. Mann, *Nano Lett.* **2003**, *3*, 413–417.
[19] J.-S. Lim, S.-M. Kim, S.-Y. Lee, E. A. Stach, J. N. Culver, M. T. Harris, *J. Nanomater.* **2010**, *2010*, 1–7.

[20] a) J. M. Alonso, M. Ł. Górzny, A. M. Bittner, *Trends Biotechnol.* **2013**, *31*, 530 – 538; b) A. M. Bittner, J. M. Alonso, M. L. Gorzny, C. Wege, *Subcell. Biochem.* **2013**, *68*, 667 – 702; c) Z. Liu, J. Qiao, Z. Niu, Q. Wang, *Chem. Soc. Rev.* **2012**, *41*, 6178 – 6194;d) G. Lomonossoff, D. Evans, in *Plant Viral Vectors, Vol. 375* (Eds.: K. Palmer, Y. Gleba), Springer, Berlin/Heidelberg, **2014**, pp. 61 – 87.
[21] R. Coppage, M. R. Knecht, in *Bio-Inspired Nanotechnology* (Eds.: M. R. Knecht, T. R. Walsh), Springer, New York, **2014**, pp. 173 – 219.
[22] K. Namba, G. Stubbs, *Science* **1986**, *231*, 1401 – 1406.
[23] a) H. Yi, S. Nisar, S. Lee, M. A. Powers, W. E. Bentley, G. F. Payne, R. Ghodssi, G. W. Rubloff, M. T. Harris, J. N. Culver, *Nano Lett.* **2005**, *5*, 1931 – 1936; b) S. Lee, E. Royston, J. N. Culver, M. T. Harris, *Nanotechnology* **2005**, *16*, S435 – S441.
[24] J.-S. Lim, S.-M. Kim, S.-Y. Lee, E. A. Stach, J. N. Culver, M. T. Harris, *J. Colloid Interface Sci.* **2010**, *342*, 455 – 461.
[25] A. K. Manocchi, N. E. Horelik, B. Lee, H. Yi, *Langmuir* **2010**, *26*, 3670 – 3677.
[26] A. K. Manocchi, S. Seifert, B. Lee, H. Yi, *Langmuir* **2010**, *26*, 7516 – 7522.
[27] A. K. Manocchi, S. Seifert, B. Lee, H. Yi, *Langmuir* **2011**, *27*, 7052 – 7058.
[28] C. Yang, A. K. Manocchi, B. Lee, H. Yi, *Appl. Catal. B* **2010**, *93*, 282 – 291.
[29] C. Yang, J. H. Meldon, B. Lee, H. Yi, *Catal. Today* **2014**, *233*, 108 – 116.
[30] C. Yang, H. M. Yi, *Biochem. Eng. J.* **2010**, *52*, 160 – 167.
[31] A. Suzuki, *J. Organomet. Chem.* **1999**, *576*, 147 – 168.
[32] C. Yang, A. K. Manocchi, B. Lee, H. Yi, *J. Mater. Chem.* **2011**, *21*, 187 – 194.
[33] C. Röhlich, A. S. Wirth, K. Köhler, *Chem. Eur. J.* **2012**, *18*, 15485 – 15494.
[34] H. Lakmini, I. Ciofini, A. Jutand, C. Amatore, C. Adamo, *J. Phys. Chem. A* **2008**, *112*, 12896 – 12903.
[35] H. Sakurai, T. Tsukuda, T. Hirao, *J. Org. Chem.* **2002**, *67*, 2721 – 2722.
[36] L. Artok, H. Bulut, *Tetrahedron Lett.* **2004**, *45*, 3881 – 3884.
[37] S. S. Yi, D. H. Lee, E. Sin, Y. S. Lee, *Tetrahedron Lett.* **2007**, *48*, 6771 – 6775.
[38] a) N. T. S. Phan, M. Van Der Sluys, C. W. Jones, *Adv. Synth. Catal.* **2006**, *348*, 609 – 679; b) A. Gaikwad, A. Holuigue, M. Thathagar, J. Elshof, G. Rothenberg, *Chem. Eur. J.* **2007**, *13*, 6908 – 6913; c) J. P. Simeone, J. R. Sowa Jr, *Tetrahedron* **2007**, *63*, 12646 – 12654.
[39] D. Dendukuri, P. S. Doyle, *Adv.Mater.* **2009**, *21*, 4071 – 4086.
[40] C. L. Lewis, Y. Lin, C. Yang, A. K. Manocchi, K. P. Yuet, P. S. Doyle, H. Yi, *Langmuir* **2010**, *26*, 13436 – 13441.
[41] a) J.-S. Lim, S.-M. Kim, S.-Y. Lee, E. A. Stach, J. N. Culver, M. T. Harris, *Nano Lett.* **2010**, *10*, 3863 – 3867; b) J.-S. Lim, S.-M. Kim, S.-Y. Lee, E. A. Stach, J. N. Culver, M. T. Harris, *J. Colloid Interface Sci.* **2011**, *356*, 31 – 36.
[42] C. Yang, C.-H. Choi, C.-S. Lee, H. Yi, *ACS Nano* **2013**, *7*, 5032 – 5044.
[43] C. Yang, S. Jung, H. Yi, *Biochem. Eng. J.* **2014**, *89*, 10 – 20.
[44] M. Sarikaya, C. Tamerler, A. K. Y. Jen, K. Schulten, F. Baneyx, *Nat. Mater.* **2003**, *2*, 577 – 585.
[45] D. Oh, J. Qi, B. Han, G. Zhang, T. J. Carney, J. Ohmura, Y. Zhang, Y. Shao-Horn, A. M. Belcher, *Nano Lett.* **2014**, *14*, 4837 – 4845.

Received: April 5, 2015
Published online on June 23, 2015